Analysis of 2D Unsteady Flow Past a Square Cylinder at Low Reynolds Numbers with CFD and a mesh refinement method

ZHENQUAN LI
School of Computing and Mathematics
Charles Sturt University
Albury-Wodonga Campus, NSW 2640
AUSTRALIA
jali@csu.edu.au   http://csusap.csu.edu.au/~jali/

Abstract: - A study of the behaviour of flow past a square cylinder for Reynolds numbers 10 and 20 is conducted with open source software Navier2d in Matlab and an adaptive mesh refinement method. The investigation starts from a uniform initial mesh and then refine the initial mesh using the adaptive mesh refinement method and the finite volume method implemented in Navier2d. The horizontal and vertical velocity component profiles, pressures and the velocity quiver are shown on the once refined meshes. The accuracy of the quiver plots on once refined mesh are examined by comparing them with the quiver plots on a finer mesh and considering the symmetry of the velocity fields and other characteristics.

Key-Words: - adaptive mesh refinement method, square cylinder, Reynolds number, finite volume method, CFD, Navier2D

1 Introduction

The study on wakes of flow around a bluff body has various applications in practice such as aerodynamics, wind engineering, and electronics cooling. The flow around a circular or square cylinder has been investigated extensively using different methods in literature [e.g. 1, 2, 11, 12, 13, 14].

We use a different computational technique to analyse the flow past a square cylinder. A 2D adaptive mesh refinement method is proposed based on the qualitative theory of differential equations [4]. The adaptive mesh method combines both qualitative properties of differential equations and quantitative/numerical methods for partial differential equations. The accuracy of the method is verified by analytical and CFD velocity fields considering the location of centres of vortices and/or separating curves of different vortex regions [5, 6, 8, 9]. The reliability of the method is considered and the positive outcome had been achieved [7]. The cost (computational complexity) is investigated using lid-driven cavity flow and a positive outcome again is achieved [10]. We use Navier2d as the numerical method in this paper. Navier2d is a vertex centred Finite Volume (FV) code that uses the median dual mesh for the Control Volumes (CV's) about each vertex. One of the advantages of the adaptive mesh refinement method is that a mesh is refined based on the information of the calculated velocity field on the mesh so the refined mesh shows where the velocity is more complex which is presented by more nodes in the refined mesh.

In this paper, we apply the adaptive mesh refinement once to the initial mesh. We show the velocity fields and pressures calculated on the once refined mesh, and the twice refined meshes that provide the information in the areas where the "qualitative" accuracy is not enough [9].

2 The Governing Equations

In this paper, we use Navier-Stokes equations for unsteady flow of an incompressible fluid of density as governing equations.

$$\frac{\partial \boldsymbol{u}}{\partial t} + \boldsymbol{u} \cdot \nabla \boldsymbol{u} = -\nabla p + \frac{1}{Re} \nabla^2 \boldsymbol{u}$$

$$\nabla \cdot \boldsymbol{u} = 0$$

(1)

where Re is the Reynolds number.

The domain in this study is a rectangle with the length 30 units and width 10 units as shown in Fig. 1. The unit square cylinder is placed inside of the rectangle with the centre located at (10.5, 5). The flow is from top to bottom. The origin of the xy coordinate system is located at the lower top-left corner of the rectangle and the x axis is in the downstream direction. For free stream condition

($u = 1$ and $v = 0$) at the inlet, the necessary distance from the computational inlet to the cylinder for obtaining results independent of this inlet location is about 10 units [2, 15].
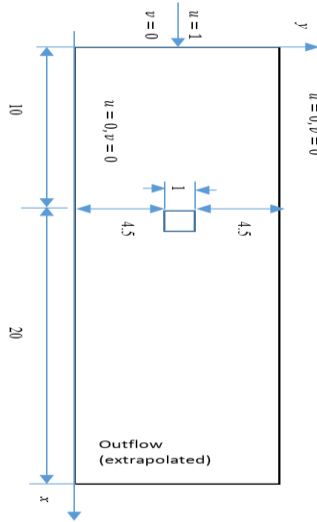

Fig. 1. Computational domain.

The boundary condition at the inlet is the free stream condition. On the left and right boundaries of the rectangle and the boundary of the square cylinder $u = v = 0$. The boundary condition at the outlet is the outflow extrapolate chosen from the options in Navier2d.

3 Numerical results

We solve the governing equations by software Navier2D on the initial mesh and then apply the adaptive mesh refinement method using the numerical velocity field calculated on the initial mesh to the initial mesh to refine the cells where the mesh refinement criteria are satisfied. We analyze the velocity fields obtained from the once refined mesh. The twice refined meshes are also shown.

3.1 The algorithm of adaptive mesh refinement

For a given discrete vector field at the three vertices of a triangle, a continuous vector field on the triangle $\mathbf{V}_l = \mathbf{AX} + \mathbf{b}$ is obtained by linearly interpolating the vectors at the three vertices of the triangle, where

$$\mathbf{A} = \begin{pmatrix} a_{11} & a_{12} \\ a_{21} & a_{22} \end{pmatrix}$$

is a matrix of constants,

$$\mathbf{b} = \begin{pmatrix} b'_1 \\ b'_2 \end{pmatrix}$$

is a vector of constants, and $\mathbf{X} = (x_1, x_2)^T$. The continuity equation for $\mathbf{V}_l$ and an incompressible fluid in Eq. (1) becomes

$$\nabla \cdot \mathbf{V}_l = \text{trace}(\mathbf{A}) = 0. \tag{2}$$

Let f be a scalar function depending only on spatial variables x_1 and x_2. We assume that $f\,\mathbf{V}_l$ satisfies the continuity equation in Eq. (1) and then calculate the expression of f. The expressions of f were derived for the four different Jacobean forms of the coefficient matrix $\mathbf{A}$ as shown in Table 1 [4]. Variables y_1 and y_2 in Table 1 are the coordinates of $(y_1, y_2)^T = \mathbf{V}^{-1}\mathbf{X}$ where $\mathbf{V}$ satisfies $\mathbf{AV} = \mathbf{VJ}$ and $\mathbf{J}$ is one of the Jacobian matrices in Table 1. b_1 and b_2 in Table 1 are the coordinates of $(b_1, b_2)^T = \mathbf{V}^{-1}\mathbf{b}$.

TABLE 1: Jacobian matrices and corresponding expressions of f ($C \neq 0$)

Case	Jacobean	f
1	$\begin{pmatrix} r_1 & 0 \\ 0 & r_2 \end{pmatrix}$ $(0 \neq r_1 \neq r_2 \neq 0)$	$\dfrac{C}{\left(y_1 + \frac{b_1}{r_1}\right)\left(y_2 + \frac{b_2}{r_2}\right)}$
2	$\begin{pmatrix} r_1 & 0 \\ 0 & 0 \end{pmatrix}$ $(r_1 \neq 0)$	$\dfrac{C}{y_1 + \frac{b_1}{r_1}}$
3	$\begin{pmatrix} r & 1 \\ 0 & r \end{pmatrix}$ $(r \neq 0)$	$\dfrac{C}{y_2 + \frac{b_2}{r}}$
4	$\begin{pmatrix} \mu & \lambda \\ -\lambda & \mu \end{pmatrix}$ $(\mu \neq 0, \lambda \neq 0)$	$\dfrac{C}{\left(y_1 + \frac{\mu b_1 - \lambda b_2}{\mu^2 + \lambda^2}\right)^2 + \left(y_2 + \frac{\lambda b_1 + \mu b_2}{\mu^2 + \lambda^2}\right)^2}$

We describe the adaptive mesh refinement algorithm by introducing the algorithm for cell refinement first [4]. The refinement conditions (MC) are that $f \neq \infty$ and $f \neq 0$ on a triangle. The algorithm of cell refinement is:

Step 1 Subdivide a quadrilateral cell into two triangles. If $\mathbf{V}_l$ satisfies Eq. (2) on both triangles, no refinement for the cell is required. Otherwise, go to Step 2;

Step 2 Apply the conditions (MC) to both of the triangles. If the conditions (MC) are satisfied on both triangles, no refinement for the cell is required. Otherwise, we subdivide the cell into a number of smaller cells such that the lengths of all sides of the smaller cells are truly reduced (e.g. connecting the mid-points of opposite sides of a quadrilateral by line segments produces four smaller quadrilaterals and the lengths of all sides of the four smaller quadrilaterals are truly reduced).

The algorithm of adaptive mesh refinement is:

Step 1 Evaluate the numerical velocity field for a given initial mesh;

Step 2 Refine all cells of the initial mesh one by one using the above algorithm of cell refinement;

Step 3 Take the refined mesh as initial mesh and go to Step 1 until a satisfactory numerical velocity field is obtained or the threshold number T is reached.

In this paper, we use the subdivision of a quadrilateral cell by connecting the mid-points of two opposite sides of a quadrilateral. We start from the uniform initial mesh with size 20×60 or the step size is half units for both x and y directions. The initial mesh is refined based on the CFD velocity field calculated on the initial mesh. We then calculate the CFD velocity field on the once refined mesh. From the once refined mesh, we obtain the information about where the linearly interpolated velocity field does not follow the equivalent continuity equation [4]. We consider the cases for Reynolds number $Re = 10$ and 20. Fig. 2 shows the initial mesh.
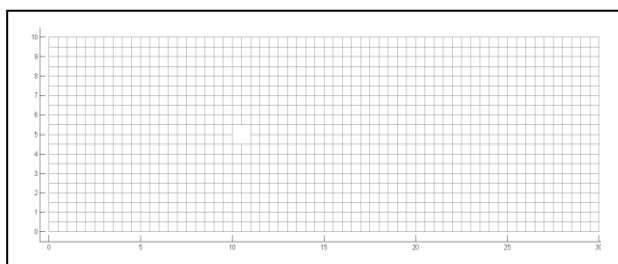

Fig. 2. Initial mesh used in study.

Navier2d requires the triangular mesh in the calculations. Fig.3 shows the triangular mesh generated from the initial mesh.
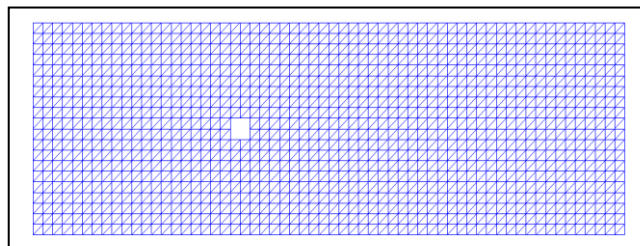

Fig. 3 Triangular mesh generated from the initial mesh.

The calculations reported in this paper have residuals for both x and y directions are less than 10^{-15}.

3.2 Once refined meshes

Fig. 4 shows the once refined meshes. The top figure is the refined mesh for $Re = 10$ and the bottom is for $Re = 20$. The setting for the flows in this study is symmetric but the refined meshes are not. That indicates that the calculated velocity fields are not symmetrical so they are not accurate enough. The cells around the cylinder and those behind the cylinder are refined.
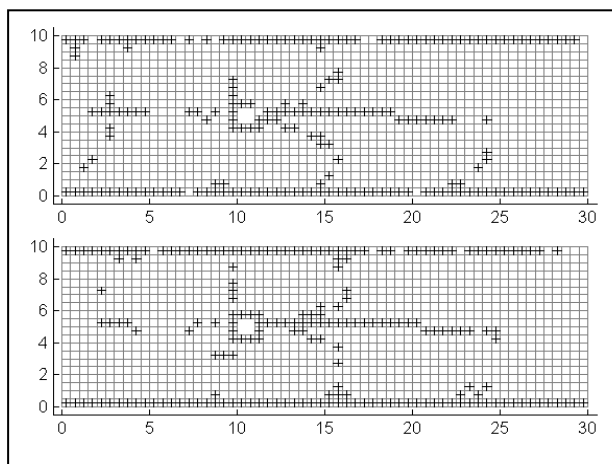

Fig. 4. The once refined meshes $Re = 10$ and 20.

3.3 u velocities

The following figures present the differences of velocity components u for $Re = 10$ and $Re = 20$ between the initial and once refined meshes.

The top plots in Figs. 5 and 6 are u profiles on the initial mesh and the bottom plots are the profiles on once refined mesh for both $Re = 10$ and 20. The both bottom plots show more details around the cylinder and the entrance. The last section will show

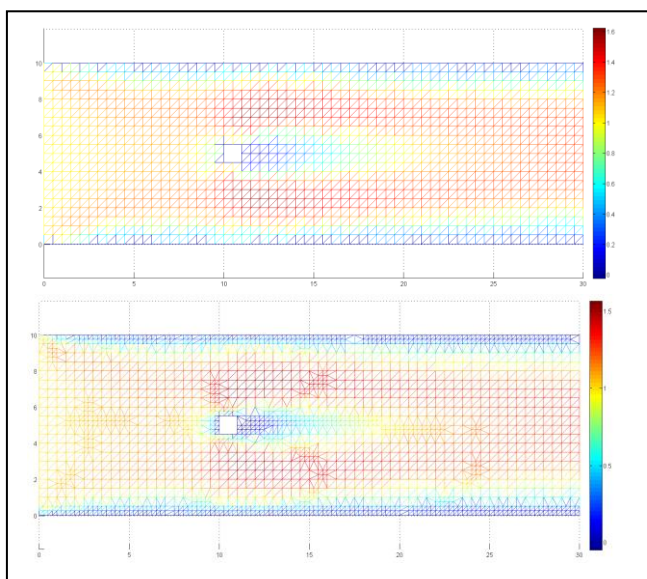that the profiles on once refined mesh are more accurate than those on the initial mesh.

Fig. 5. The profiles of u components for $Re = 10$.

In Fig. 5, the width of region where the magnitude of u is less 0.5 behind the cylinder on the initial mesh is wider than that on the refined mesh. The wake behind cylinder is longer in the top figure than that in the bottom figure.
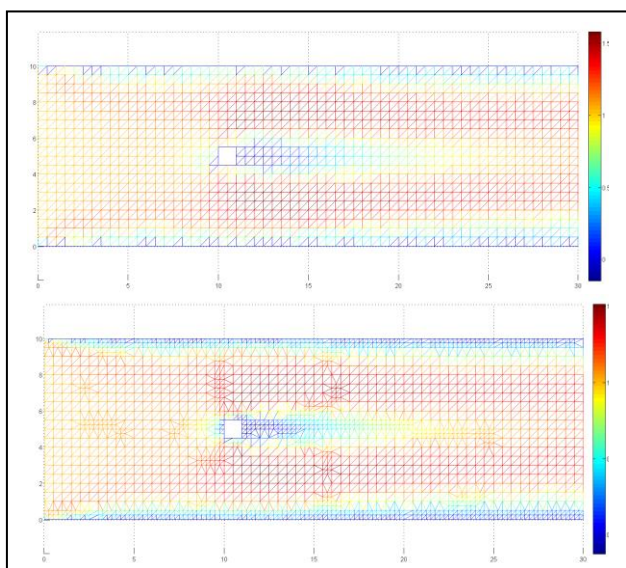

Fig. 6. The profiles of u components for $Re = 20$.

In Fig. 6, the width of region where the magnitude of u is less 0.5 behind the cylinder on the initial mesh is similar to that on the refined mesh. The wake behind cylinder on the initial mesh is also similar to that on the refined mesh.

3.4 v velocities

This section shows the differences of vertical velocity components v for $Re = 10$ and $Re = 20$ between the initial and once refined meshes.

The same settings as in Figs. 5 and 6 are arranged in Figs. 7 and 8. v profiles on the initial mesh and once refined mesh have much less variations than those of u.
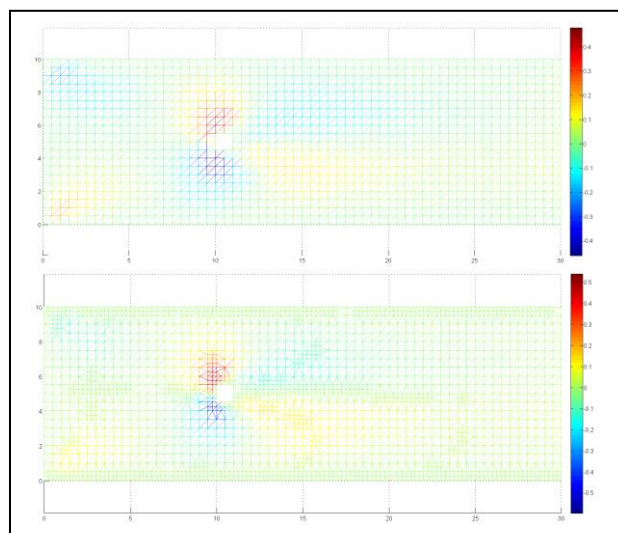

Fig. 7. The profiles of v components for $Re = 10$.

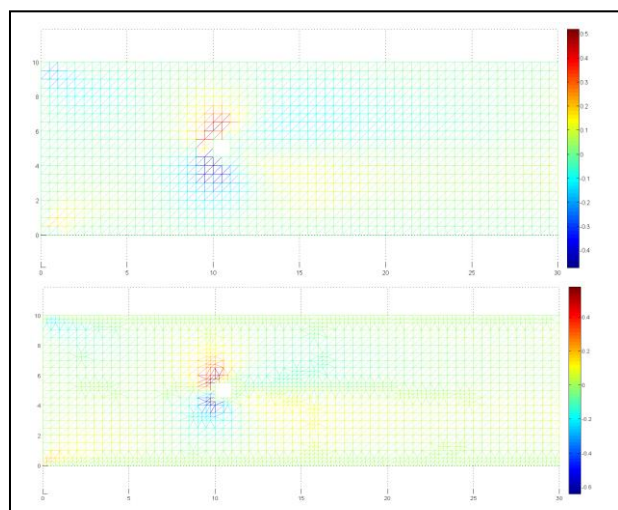In Fig. 7 for $Re = 10$, both plots show non symmetrical but the refined mesh is improving.

Fig. 8. The profiles of v components for $Re = 20$.

In Fig. 8, both plots also show non symmetrical but the refined mesh is improving.

3.5 Pressure comparison
The comparisons of pressures for both $Re = 10$ and $Re = 20$ are shown in Figs. 9 and 10, respectively.

There are large differences between the pressures on the initial and once refined meshes for $Re = 10$. The pressure before the cylinder is larger for Re=10 than that of the case Re=20 since the flow is faster in the latter case.
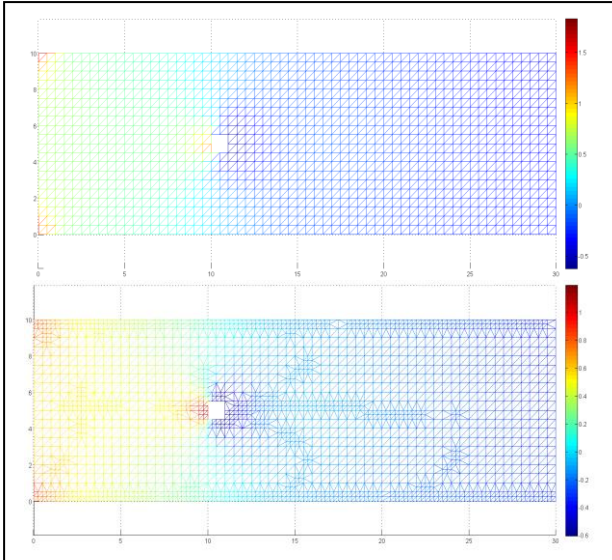

Fig. 9. Pressure profiles for $Re = 10$.

Since same amount of fluids comes into the channel at the entrances, the pressure for $Re = 10$ is larger than that for $Re = 20$. Therefore, the pressure profiles for both $Re = 10$ and $Re = 20$ are correct on the initial meshes. However, the pressure profiles on the once refined meshes show different information. The pressure shown on the once refined mesh for $Re = 10$ in Fig. 9 is larger before the cylinder and smaller in adjacent area just behind cylinder than those on the initial mesh.
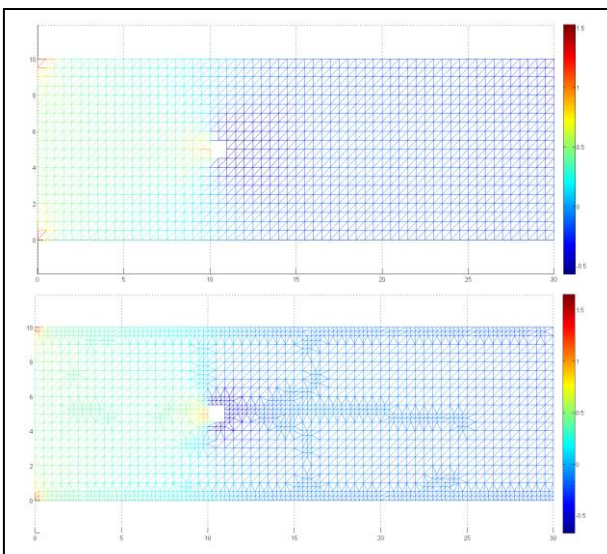

Fig. 10. Pressure profiles for $Re = 20$.

Even though the pressure variation for $Re = 20$ shown in Fig. 10 is similar to that for the case for $Re = 10$ before and behind the cylinder on the initial and once refined meshes, the magnitude is much smaller.

3.6 Velocity fields

Figs. 11 and 12 show the quiver plots of velocity fields calculated from Navier2d on the initial (top graph), once refined mesh (middle graph) and a uniform mesh which subdivides each cell of the initial mesh (bottom graph) into four equal smaller cells for both $Re = 10$ and $Re = 20$. For both cases in Figs. 10 and 20, the accuracy is getting better and better from top to bottom. The wakes after the cylinder for both cases are a little bit shorter on the once refined meshes than those of the bottom graphs. However, the patterns before and around the cylinder are improved very much, especially the areas just behind the cylinder on once refined meshes.
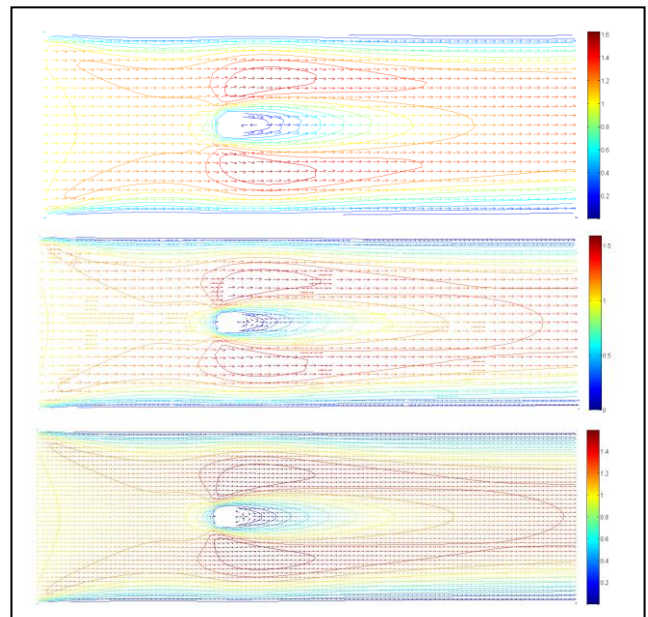

Fig. 11. Quiver plot of velocity fields for $Re = 10$.

In Fig. 11 for $Re = 10$, the plot on the once refined mesh improves very much at the inlet, in the areas surrounding the cylinder and of the wake from the plot on the initial mesh. The non-symmetrical profile of the velocity field is obviously shown around the inlet on the top plot but in the once refined mesh, this has been improved. Even though the velocity field profile looks symmetrical at the top and bottom of the cylinder and behind cylinder on the initial mesh, the details just behind the cylinder is not provided enough. However, the

profiles at the top and bottom of the cylinder in the middle plot is not symmetrical.
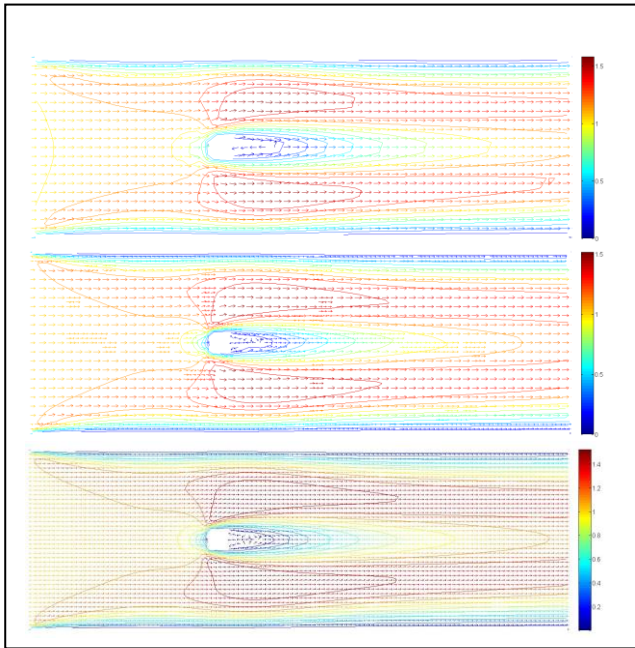

Fig. 12. Quiver plot of velocity fields for $Re = 20$.

In Fig. 12 for $Re = 20$, the plot on the once refined mesh improves at the inlet, in the areas surrounding the cylinder and of the wake from the plot on the initial mesh. The non-symmetrical profile of the velocity field is shown around the inlet at the top plot, in the areas of the top and bottom of cylinder and the wake on the initial mesh but on the once refined mesh, these areas have been improved. The velocity field profile looks not symmetrical at the top and bottom of the cylinder and in the wake on the initial mesh, the details just behind the cylinder is not enough. The velocity field profile in the middle plot looks symmetrical but there are still differences in the wake regions between the middle and the bottom plots.

3.7 More mesh refinements

If the information provided on once refined meshes are not accurate enough, more refinements can be performed until satisfactory results are obtained following the algorithm in Section 3.1. Even though the information provided on once refined meshes are not exactly the same as that on the mesh with double size of the initial mesh, the symmetry of and the accuracy of velocity fields and pressures have been improved very much comparing with the outputs on the initial meshes as shown in Fig. 13 (taking the velocity for $Re = 10$ as an example) There are only 2025 nodes on the once refined mesh (including those on the boundary) for $Re = 10$ and 2079 nodes on the once refined mesh for $Re = 20$.
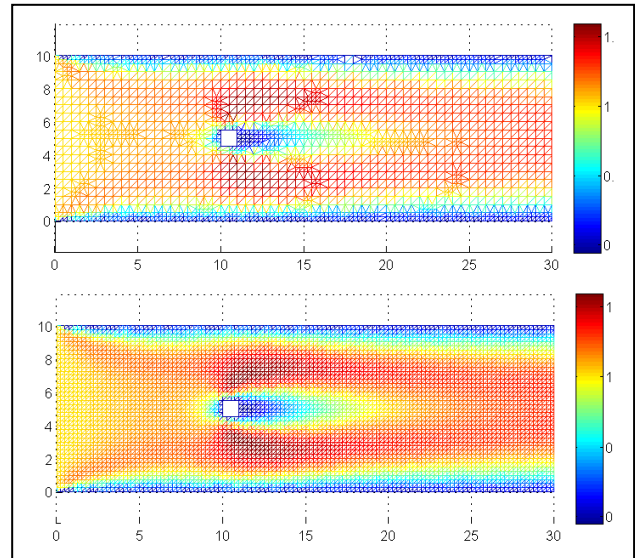

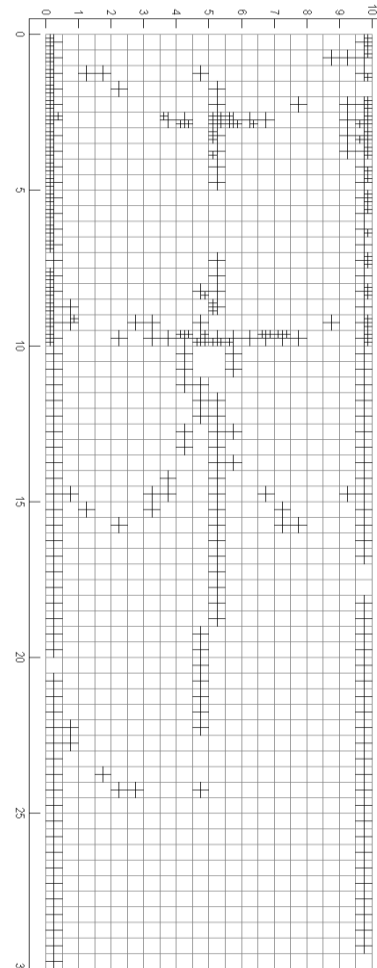**Fig. 13.** The profiles of u on once refined and 40 by 40 uniform meshes for $Re = 10$.

Fig. 14. Twice refined mesh for $Re = 10$.

The computational complexities for the calculations of the velocity fields and pressures on once refined mesh are much less than that on the mesh with double size of the initial mesh which has 4952

nodes [10]. This can be also obtained from the once refined meshes in Fig. 4.

Since we select the boundaries manually for setting the boundary conditions using Navier2D, it is difficult to select those nodes exactly on the boundaries only as shown in the enlarged twice refined meshes Figs. 14 and 15. The more refined meshes, and velocity fields and pressures on them are impossible to present here. Other software have to be used if more accurate results for velocity fields and pressures are required.
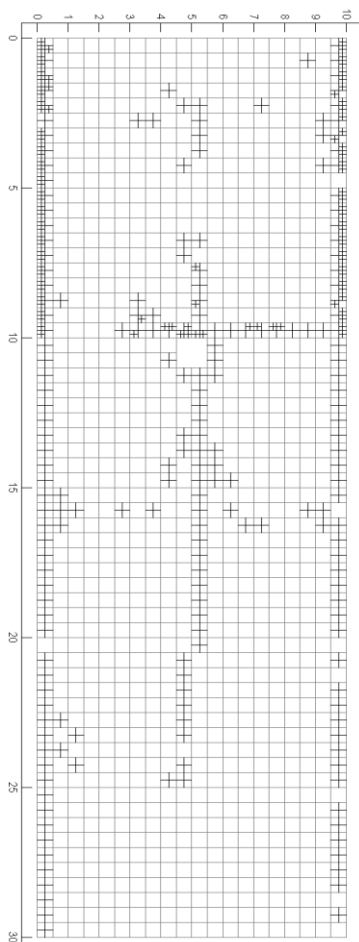

Fig. 15. Twice refined mesh for $Re = 20$.

4 Conclusion

We have shown the information about velocity fields, pressure and quiver plots of the flow passing through a square cylinder in this paper. The boundary conditions used in this paper are different from the boundary conditions used in [1, 2]. We use the adaptive mesh refinement method in the analysis of the flow for $Re = 10$ and $Re = 20$.

In the future, we will consider improving the accuracy of the numerical velocity fields in two ways. The first way is to choose finer initial mesh

and the second is the use of a different CFD software and perform more refinements on the initial mesh. When the size of initial mesh is getting bigger, the selection of the nodes exactly on the segments of the boundary becomes more difficulty when we use Navier2D. The choice of which one of the two ways are totally depending on the required accuracy.

References:
[1] S. Sen, S. Mittal, G. Biswas, Flow past a square cylinder at low Reynolds numbers, *Int. J. Numer. Meth. Fluids,* Vol. 67, 2011, pp. 1160-1174. DOI : 10.1002/fld.2416
[2] B. Gera, P.K. Sharma, P.K. Singh, CFD analysis of 2D unsteady flow around a square cylinder, *Int. J. Appl. Eng. Res.*, Vol. 1, 602-610(2010). http://ipublishing.co.in/jarvol1no12010/EIJAER2028.pdf
[3] D. Engwirda, *Navier–Stokes solver (Navier2d).* MATLAB Central File Exchange, 2006.
[4] Z. Li, An adaptive two-dimensional mesh refinement method based on the law of mass conservation, *J. Flow Visual. Image Process.*, Vol. 15, No. 1, 2008, pp. 17-33. DOI: 10.1615/JFlowVisImageProc.v15.i1.20
[5] Z. Li, An adaptive streamline tracking method for two-dimensional CFD velocity fields based on the law of mass conservation, *J. Flow Visual. Image Process.*, Vol. **13**, No. 1, 2006, pp. 1-14. DOI: 10.1615/JFlowVisImageProc.v13.i1.10
[6] Z. Li, Accuracy analysis of a mesh refinement method using benchmarks of 2-D lid-driven cavity flows and finer meshes, *J. Math. Chem.*, Vol. 52, No. 4, 2014, pp. 1156-1170. DOI : 10.1007/s10910-014-0334-0
[7] R. Lal, Z. Li, Sensitivity analysis of a mesh refinement method using the numerical solutions of 2D lid-driven cavity flow, *J. Math. Chem.*, Vol. 53, No. 3, 2015, pp. 844-867. DOI: 10.1007/s10910-014-0461-7
[8] Z. Li, R. Wood, Accuracy analysis of an adaptive mesh refinement method using benchmarks of 2-D steady incompressible lid-driven cavity flows and coarser meshes, *J. Comput. Appl. Math.*, Vol. 275, No. 10, 2015, pp. 262-271. DOI: 10.1016/j.cam.2014.07.025
[9] Z. Li, R. Wood, Accuracy verification of a 2D adaptive mesh refinement method for incompressible or steady flow, *J. Comput. Appl. Math.*, Vol. 318, No. 7, 2017, pp. 259-265. DOI: 10.1016/j.cam.2016.09.022

[10] Z. Li, Computational complexity of the algorithm for a 2D adaptive mesh refinement method using lid-driven cavity flows, *Comput. Therm. Sci.*, No. 5, Vol. 9, 2017, pp. 395-403.

[11] A. Pantokratoras, Unconfined unsteady laminar flow of a power-law fluid across a square cylinder, *Fluids*, No. 4, Vol. 1: 37, 2016, doi:10.3390/fluids1040037

[12] S. Sen, S. Mittal, G. Biswas, Steady separated low past a circular cylinder at low Reynolds numbers, *J. Fluid Mech.,* Vol. 620, 2009, pp. 89-119.

[13] R.W. Davis, E.F. Moore, L.P. Purtell, A numerical-experimental study of confined flow around rectangular cylinders, Physics of Fluids, Vol. 27, 1984, pp. 46-59.

[14] W. Zhang, Y.Q. Jiang, L. Li, G.P Chen, Effects of wall suction/blowing on two‑dimensional flow past a confined square cylinder, *SpringerPlus*, Vol. 5: 985, 2016, doi 10.1186/s40064-016-2666-7

[15] A. Sohankar, C. Norberg, L. Davidson, Low-Reynoolds number flow around a square cylinder at incidence: study of blockage, onset of vortex shedding and outlet boundary condition, *Int. J. Numer. Methods Fluids*, Vol. 26, 1998, pp. 39-56.